FOPID-Based Trajectory Control for an Unmanned Aerial Robotic Manipulator

Keywords: Aerial Manipulators, Fractional-Order PID, FOPID Control, UMA, Trajectory Tracking, UAV-Based

Manipulation.

Abstract: This work presents a Fractional Order PID (FOPID) control strategy for trajectory tracking of an Unmanned

Aerial Manipulator (UAM), proposed as an alternative to the conventional PID controller. Unlike classical integer-order controllers, the FOPID design enables more flexible tuning of the aerial manipulator's kinematic response by introducing five independent tuning parameters. This added flexibility enhances system stability and improves robustness against abrupt reference changes. The controller parameters are optimized through Integral of Squared Error (ISE) minimization to ensure efficient performance. Simulation results confirm that the FOPID controller achieves superior trajectory tracking accuracy compared to the conventional PID. Specifically, the ISE values obtained with the FOPID reflect reductions of 23.46%, 24.99%, and 15.35% in the tracking errors along the \tilde{x} , \tilde{y} and \tilde{z} directions, respectively. These results validate the effectiveness of the

FOPID approach in improving the control performance of unmanned aerial manipulators.

1 INTRODUCTION

Unmanned Aerial Manipulators (UAMs) integrate the mobility of Unmanned Aerial Vehicles (UAVs) with the manipulation capabilities of robotic arms, posing significant control challenges due to their high nonlinearities, strong couplings, and external disturbances. Although full dynamic models offer accuracy (Carvajal et al., 2024), their complexity restricts real-time implementation. Consequently, some approaches adopt decoupled dynamics (Sharma et al., 2025), (Zhang et al., 2021) or treat the robotic arm as a disturbance (Zheng et al., 2023). Within this framework, kinematic models offer a suitable alternative for achieving precise trajectory tracking at low computational cost, particularly in low-speed operation scenarios.

Classical integer-order PID controllers have been extensively applied in robotics due to their simplicity and ease of implementation (Moya et al., 2016; Mundheda et al., 2023), but they exhibit significant

limitations when dealing with external disturbances, parametric variations, and nonlinearities (Leica et al., 2017), especially in systems such as UAMs. To address these shortcomings, various PID extensions have been proposed, including adaptive schemes (Ghamari et al., 2022), sliding mode controllers (Noordin et al., 2022), fuzzy logic-based controllers (Cao et al., 2022), and sigmoid-based control structures (Suid & Ahmad, 2022). Nonetheless, all of these strategies still operate under the constraints of integer-order dynamics.

Fractional-order control theory generalizes the classical PID framework by allowing non-integer orders in the integral and derivative operators, thus introducing two additional degrees of freedom that enhance tuning flexibility and the ability to model real-world systems more accurately (Torvik & Bagley, 1984). FOPID controllers have demonstrated superior performance in diverse robotic applications. For example, in robotic manipulators, FOPID schemes have been integrated with neural networks

alp https://orcid.org/0000-0002-1822-6943

b https://orcid.org/0009-0009-4826-9475

https://orcid.org/0000-0002-5385-1920

dip https://orcid.org/0000-0002-8408-1280

(Mohamed et al., 2023), applied in iterative modelfree control (Zhang et al., 2021), combined with sliding mode control (Noordin et al., 2022), and tuned using nature-inspired algorithms such as the Bat algorithm (A. Faraj & Mohammed Abbood, 2021) or optimization-based methods (Ghamari et al., 2022). In the UAVs, FOPID controllers have been improved tracking precision and robustness against parametric uncertainties using micro-integral operators (Delgado-Reyes et al., 2024; Li et al., 2023). Experimental comparisons with adaptive schemes further confirm their superiority over classical PID (Timis et al., 2022). In UAMs, FOPID has been combined with predictive and sliding mode control strategies, yielding significant improvements in disturbance rejection and trajectory tracking (Shao et al., 2025; Zheng et al., 2023). However, many of these approaches assume accurate knowledge of the system dynamics, which remains a practical limitation due to the inherent complexity of UAM platforms. Based on the literature, FOPID controllers have demonstrated significant advantages in precision and robustness against disturbances and uncertainties, with successful applications in aerial and ground robotics (UAVs and UGVs), particularly in scenarios with wind gusts, payload variations, friction, and model inaccuracies (Cajo et al., 2019). Nevertheless, their implementation in UAM systems remains limited, despite the high potential fractionalorder control offers for this domain.

This work proposes the design and implementation of a fractional-order PID (FOPID) controller, formulated using the Caputo fractional derivative operator, applied to the kinematic model of a UAM composed of a quadrotor and a 3-DOF robotic arm. Unlike previous approaches that rely on complex dynamic models with high real-time computational costs, the proposed method enables efficient and precise trajectory tracking control under abrupt reference changes. The results demonstrate significant improvements over classical PID controllers, exhibiting smoother and more robust responses, thereby positioning the FOPID as an effective alternative for robust kinematic control of UAMs. The main contributions of this work are: i) a novel application of FOPID control in aerial manipulators, providing a foundation for future research; and ii) a control strategy that does not require an exact system model, making it particularly suitable for platforms like UAMs, whose dynamics are complex and highly coupled.

The article is organized as follows: Section 1 presents a review of FOPID controllers and the contributions of this work; Section 2 describes the

modeling of the manipulator, the quadrotor and UAM; Section 3 details the PID and FOPID controllers along with the stability analysis; Section 4 presents the obtained results; and Section 5 summarizes the study's conclusions.

2 SYSTEM MODELING

2.1 Quadrotor Modeling

For this work, an aerial manipulator composed of a quadrotor equipped with a 3-DOF robotic arm is considered, as illustrated in Figure 1. Under the assumption of operation around equilibrium, it is assumed that the roll and pitch angles are negligible, which allows simplifying the quadrotor kinematics by considering only translations in the horizontal plane and a constant yaw orientation (Guayasamín et al., 2018).

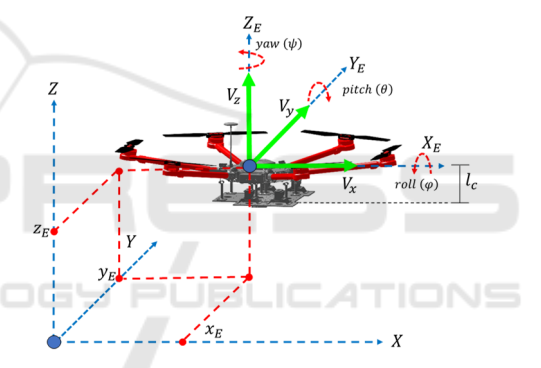


Figure 1: Quadrotor Robot.

$$\begin{bmatrix} \dot{x}_E \\ \dot{y}_E \\ \dot{z}_E \end{bmatrix} = \begin{bmatrix} \cos \psi & -\sin \psi & 0 \\ \sin \psi & \cos \psi & 0 \\ 0 & 0 & 1 \end{bmatrix} \begin{bmatrix} V_x \\ V_y \\ V_z \end{bmatrix}, \tag{1}$$

where V_x , V_y and V_z are the linear velocities of the quadrotor, $[x_E, y_E, z_E]^T$ represents the position with respect to the quadrotor's X, Y and Z axes, ψ is the rotation angle of the quadrotor about the Z-axis, and l_c is the vertical distance from the quadrotor's base to its center of mass.

2.2 Robotic Arm Modeling

A 3-DOF robotic arm is considered, as shown in Figure 2. By applying the Denavit-Hartenberg algorithm, the system's forward kinematic model is determined (Guayasamín et al., 2018), which is expressed as follows:

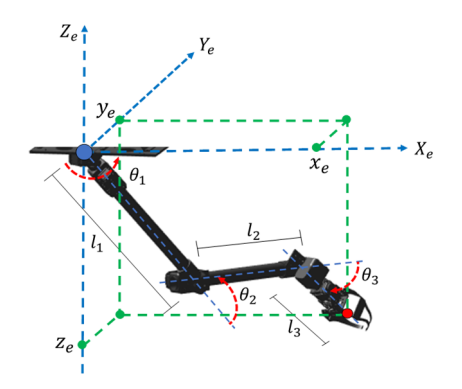


Figure 2: 3-DOF Robotic Arm.

$$\begin{bmatrix} x_e \\ y_e \\ z_e \end{bmatrix} = \begin{bmatrix} \cos \theta_1 \left[l_2 \cos \theta_2 + l_3 \cos(\theta_2 + \theta_3) \right] \\ \sin \theta_1 \left[l_2 \cos \theta_2 + l_3 \cos(\theta_2 + \theta_3) \right] \\ -l_1 \sin \theta_1 - l_2 \sin \theta_2 + l_3 \sin(\theta_2 + \theta_3) \end{bmatrix} . (2)$$

The parameters l_1 , l_2 , and l_3 denote the link lengths, θ_1 , θ_2 , and θ_3 are the joint angles, and $[x_e$, y_e , $z_e]^T$ represents the position of the manipulator's end-effector with respect to the X_e , Y_e , and Z_e axes.

2.3 Aerial Manipulator Modeling

The robotic system is formed by coupling the quadrotor with the previously described robotic arm. To obtain the combined model, it is considered that the end-effector's position is now influenced by the quadrotor's position, such that the end-effector position is given by $[x_{ee}, y_{ee}, z_{ee}]^T = [x_E + x_e, y_E + y_e, z_E + z_e + l_c]^T$, where (x_{ee}, y_{ee}, z_{ee}) denotes the position of the aerial manipulator's end-effector in X, Y, and Z axes.

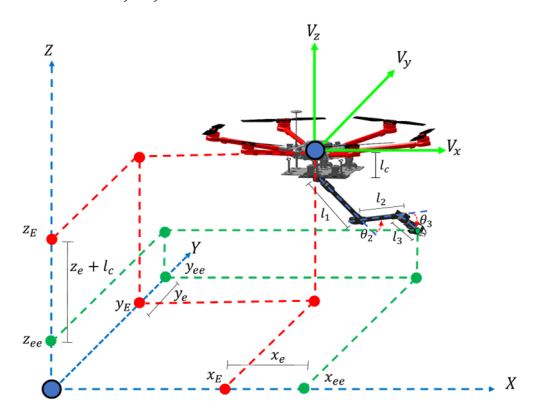


Figure 3: Unmanned Aerial Manipulator Robot.

It is considered that there exists an angle θ_a influenced by the quadrotor's yaw orientation ψ and the angle θ_1 of the first joint of the robotic arm, such

that $\theta_a = \theta_1 + \psi$. Based on these considerations, the kinematic model of the UAM is given by:

$$\dot{h} = IU, \tag{3}$$

The vector $\dot{h} = [\dot{x}_{ee}, \dot{y}_{ee}, \dot{z}_{ee}]^T$ represents the time derivative of the position of the end-effector of the aerial manipulator. The input vector of the system is defined as $U = [V_x, V_y, V_z, \dot{\psi}, \dot{\theta}_1, \dot{\theta}_2, \dot{\theta}_3]^T$ where $\dot{\psi}$ is the angular velocity of the quadrotor around the Z-axis. The angular velocities of each joint of the robotic arm are $\dot{\theta}_1$, $\dot{\theta}_2$, and $\dot{\theta}_3$.

The matrix J is the Jacobian of the complete system and is defined as:

$$J = \begin{bmatrix} C_{\psi} & S_{\psi} & 0 \\ -S_{\psi} & C_{\psi} & 0 \\ 0 & 0 & 1 \\ -S_{\theta_{1}\psi}L_{C_{23}} & C_{\theta_{1}\psi}L_{C_{23}} & 0 \\ -S_{\theta_{1}\psi}L_{C_{23}} & C_{\theta_{1}\psi}L_{C_{23}} & 0 \\ -C_{\theta_{1}\psi}L_{S_{23}} & -S_{\theta_{1}\psi}L_{S_{23}} & L'_{C_{23}} \\ -l_{3}C_{\theta_{1}\psi}S_{\theta_{2}\theta_{3}} & -l_{3}S_{\theta_{1}\psi}C_{\theta_{2}\theta_{3}} & l_{3}C_{\theta_{2}\theta_{3}} \end{bmatrix}. \quad (4)$$

The equivalent nomenclature is $C_{\psi}=\cos\psi$, $S_{\psi}=\sin\psi$, $S_{\theta_1\psi}=\sin(\theta_1+\psi)$, $C_{\theta_2}=\cos\theta_2$, $S_{\theta_2}=\sin\theta_2$, $C_{\theta_2\theta_3}=\cos(\theta_2+\theta_3)$, $C_{\theta_1\psi}=\cos(\theta_1+\psi)$, $S_{\theta_2\theta_3}=\sin(\theta_2+\theta_3)$, $L_{C_{23}}=l_2C_{\theta_2}+l_3C_{\theta_2\theta_3}$, and $L'_{C_{23}}=-l_2C_{\theta_2}+l_3C_{\theta_2\theta_3}$.

3 CONTROLLERS

This section analyzes the stability of the control laws using Lyapunov functions. The tracking error is defined as $\tilde{h} = h_d - h$, where $h = [x_{ee}, y_{ee}, z_{ee}]^T$ represents the actual position of the end-effector, and $h_d = [x_d, y_d, z_d]^T$ denotes the desired position of the end-effector, which may vary over time.

3.1 PID Controller

The classical PID control scheme is illustrated in Figure 4.

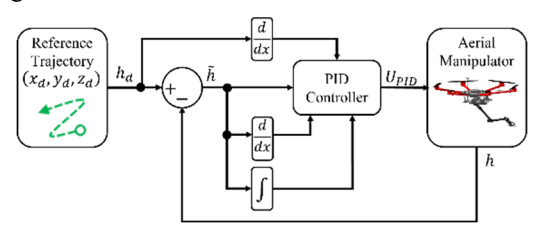


Figure 4: PID Control Scheme.

A PID-type control law is proposed for trajectory tracking of the UAM (Li et al., 2023), given by:

$$U_{PID} = J^{\#} \left(\dot{h}_{d} + k_{p} \tilde{h} + k_{i} \int \tilde{h} dt + k_{d} \dot{\tilde{h}} \right). \tag{5}$$

The gains $k_p, k_i, k_d > 0$ represent the PID controller parameters, respectively, and $\tilde{h} = h_d - h$ is the tracking error. Defining the integral term as $z = \int \tilde{h} \, dt$, with $\dot{z} = \tilde{h}$, the above expression can be rewritten as:

$$U_{PID} = J^{\#} \left(\dot{h}_d + k_p \tilde{h} + k_i z + k_d \dot{\tilde{h}} \right). \tag{6}$$

The time derivative of the tracking error is $\dot{h} = \dot{h}_a - \dot{h}$, and combining this with the kinematic model (3), we obtain:

$$\dot{\tilde{h}} = \dot{h}_d - JU. \tag{7}$$

Assuming perfect velocity tracking, i.e., $U = U_{PID}$, and substituting (6) into (7), the closed-loop system becomes:

$$\dot{\tilde{h}} = -k_p \tilde{h} - k_i z - k_d \dot{\tilde{h}}. \tag{8}$$

Solving for $\dot{\tilde{h}}$, we obtain:

$$\dot{\tilde{h}} = -\frac{k_p \tilde{h} + k_i z}{(1 + k_d)},\tag{9}$$

The following Lyapunov candidate function is proposed:

$$V = \frac{1}{2}\tilde{h}^T\tilde{h} + \frac{k_i}{2(1+k_d)}z^T z.$$
 (10)

Its time derivative is given by:

$$\dot{V} = \tilde{h}^T \dot{\tilde{h}} + \frac{k_i}{(1+k_d)} z^T \dot{z}. \tag{11}$$

Substituting (9) into (11) and expanding the terms yields:

$$\dot{V} = -\frac{k_p}{1 + k_d} \tilde{h}^T \tilde{h} - \frac{k_i}{1 + k_d} \tilde{h}^T z + \frac{k_i}{1 + k_d} z^T \tilde{h}.$$
 (12)

Since $\tilde{h}^T z = z^T \tilde{h}$, the cross terms cancel out, resulting in:

$$\dot{V} = -\frac{k_p}{1 + k_d} \tilde{h}^T \tilde{h}. \tag{13}$$

This expression guarantees that \tilde{h} and z are bounded, i.e., $\tilde{h} \in L_{\infty}$ and $z \in L_{\infty}$. To demonstrate that the errors converge to zero, LaSalle's invariance principle is applied. The invariant set is defined as:

$$S = \{(\tilde{h}, z) \in \mathbb{R}^3 x \mathbb{R}^3 : \dot{V} = 0\} \to \tilde{h} = 0.$$
 (14)

Thus, $\tilde{h} = 0$, and since $\dot{z} = \tilde{h} = 0$, it follows that z = const. Therefore, the system's solutions converge to the largest invariant set contained in S, namely:

$$M = \{(\tilde{h}, z) : \tilde{h} = 0, z = const\}.$$
 (15)

Given that $\frac{k_i}{2(1+k_d)} z^T z \to const$, and considering that V is decreasing, it is concluded that $\tilde{h} \to 0$ as $t \to \infty$. This result demonstrates the asymptotic stability of the system under the proposed PID control law.

3.2 Fopid Controller

For the design of the fractional-order PID controller (FOPID), the Caputo definition is adopted (Shah & Agashe, 2016), as it enables the derivative and integral actions of the controller to be represented through fractional-order operators applied to the tracking error. The proposed control scheme is illustrated in Figure 5.

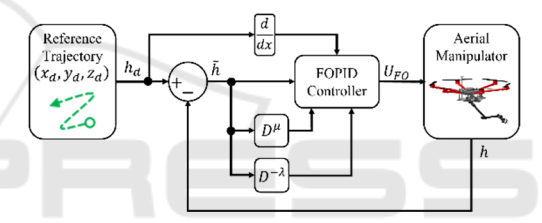


Figure 5: FOPID control scheme.

The proposed control law is defined as (A. Faraj & Mohammed Abbood, 2021):

$$U_{FO} = J^{\#} (\dot{h}_d + k_p \tilde{h} + k_i D^{-\lambda} \tilde{h} + k_d D^{\mu} \tilde{h}). \tag{16}$$

The gains $k_p, k_i, k_d > 0$ represent the PID controller parameters, and D^n denotes the fractional differential or integral operator of order n, and \tilde{h} is the tracking error. The state $z_i = D^{-\lambda}\tilde{h}$ is defined as the fractional integral of order $\lambda \in [0,1]$, such that $\tilde{h} = D^{\lambda}z_i$, while the state $z_d = D^{\mu}\tilde{h}$ corresponds to the fractional derivative of order $\mu \in [0,1]$ with $\tilde{h} = D^{1-\mu}z_d$. By substituting these expressions into (15), the control law can be rewritten as:

$$U_{FO} = J^{\#} (\dot{h_d} + k_p \tilde{h} + k_i z_i + k_d z_d). \tag{17}$$

Assuming perfect velocity tracking, we have $U = U_{FO}$. Replacing (17) into the kinematic model (3), the closed-loop dynamics are obtained as:

$$\dot{\tilde{h}} = -k_p \tilde{h} - k_i z_i - k_d z_d. \tag{18}$$

To analyze stability, the following Lyapunov candidate function is proposed:

$$V_{L} = \frac{1}{2}\tilde{h}^{T}\tilde{h} + \frac{k_{i}}{2}z_{i}^{T}z_{i} + \frac{k_{d}}{2}z_{d}^{T}z_{d}.$$
 (19)

By differentiating (19) with respect to time, we obtain:

$$\dot{V}_L = \tilde{h}^T \dot{\tilde{h}} + k_i z_i^T \dot{z}_i + k_d z_d^T \dot{z}_d. \tag{20}$$

Considering the fractional relationships:: $\dot{z}_i = \frac{d}{dt} \left(\int \tilde{h} \ dt \right) = \tilde{h} = D^{\lambda} z_i$, and $\dot{z}_d = \frac{d}{dt} \left(\tilde{h} \right) = \dot{\tilde{h}} = D^{1-\mu} z_d$; and substituting into (20), we get:

$$\dot{V}_{L} = \tilde{h}^{T} \dot{\tilde{h}} + k_{i} z_{i}^{T} D^{\lambda} z_{i} + k_{d} z_{d}^{T} D^{1-\mu} z_{d}. \tag{21}$$

Given the previously defined state variables, the Lyapunov derivative can be rewritten as:

$$\dot{V}_L = \tilde{h}^T \dot{\tilde{h}} + k_i z_i^T \tilde{h} + k_d z_d^T \dot{\tilde{h}}. \tag{22}$$

Substituting (18) into (22) and expanding, we obtain:

$$\dot{V}_{L} = -k_{p}\tilde{h}^{T}\tilde{h} - k_{d}^{2}z_{d}^{T}z_{d} - k_{d}(1 + k_{p})z_{d}^{T}\tilde{h} - k_{i}k_{d}z_{d}^{T}z_{i}.$$
(23)

Applying Young's inequality to bound the cross terms:

$$\left| z_d^T \tilde{h} \right| \le \frac{1}{2} \left(z_d^T z_d + \tilde{h}^T \tilde{h} \right). \tag{24}$$

$$|z_d^T z_i| \le \frac{1}{2} (z_d^T z_d + z_i^T z_i).$$
 (25)

Rewriting (23) in terms of inequalities, we obtain:

$$\dot{V}_{L} \leq -k_{p}\tilde{h}^{T}\tilde{h} - k_{d}^{2}z_{d}^{T}z_{d} - \frac{k_{d}}{2}(1 + k_{p})(z_{d}^{T}z_{d} + \tilde{h}^{T}\tilde{h}) - \frac{k_{i}k_{d}}{2}(z_{d}^{T}z_{d} + z_{i}^{T}z_{i}). \tag{26}$$

Developing (26) leads to:

$$\dot{V}_L \le -K_{\tilde{h}} \tilde{h}^T \tilde{h} - K_{z_d} z_d^T z_d - K_{z_i} z_i^T z_i, \tag{27}$$

where $K_{\widetilde{h}} = \left[k_p + \frac{k_d}{2}(1+k_p)\right]$, $K_{z_d} = \left[k_d^2 + \frac{k_d}{2}(1+k_p) + \frac{k_ik_d}{2}\right]$, and $K_{z_i} = \frac{k_ik_d}{2}$, are strictly positive constants.

Since $\dot{V}_L \leq 0$, the system is Lyapunov stable. Furthermore, the positivity of the coefficients guarantees that $(\tilde{h}, z_i, z_d) \rightarrow 0$ as $t \rightarrow \infty$, confirming the asymptotic convergence of the tracking error under the proposed FOPID controller.

4 TESTS AND RESULTS

This section presents the simulation results corresponding to the two proposed control algorithms: classical PID and fractional-order PID (FOPID). The objective is to compare the performance of each controller under identical operating conditions. Quantitative evaluation is carried out using the Integral of Squared Error (ISE) performance index applied to the tracking error in each coordinate of the aerial manipulator's endeffector.

The desired trajectory for the end-effector was defined as: $h_d(t) = [x_d, y_d, z_d]^T = [\cos(t/2) + 2, \sin(t/2) + 2, t/2]^T$. The simulation was run for 60 s. Additionally, to assess the controllers' adaptability to abrupt changes, a disturbance was introduced in the desired trajectory between 20 s and 40 s, consisting of a constant increment of 2 m applied to each coordinate.

Both controllers employed the same PID gains, with values $k_p=3$, $k_i=0.1$, and $k_d=1$, which were obtained through a tuning process based on the minimization of the ISE index. For the FOPID controller, the fractional orders λ and μ , associated with the integral and derivative actions respectively, were incorporated. These values were selected using heuristic methods aimed at improving performance relative to the classical PID. The values used were $\lambda=0.1$ and $\mu=0.8$. Under these conditions, simulations were conducted for both control schemes, comparing the tracking errors and the resulting ISE indices across the three coordinates.

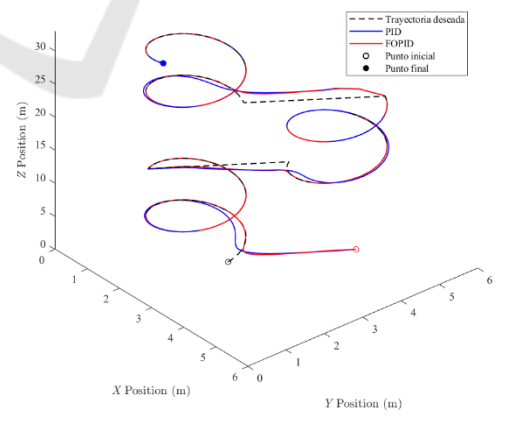


Figure 6: End-Effector Trajectory under PID and FOPID Control.

Figure 6 shows the evolution of the end-effector trajectories under classical PID and FOPID control, compared to the desired trajectory. It can be observed that both controllers are capable of achieving the

desired trajectory; however, the FOPID exhibits faster convergence and a smoother response, especially when facing abrupt changes in the reference.

Figure 7 depicts the temporal evolution of the position error in each coordinate of the end-effector under classical PID and FOPID control. The errors are displayed within a bounded range of ± 0.3 m to facilitate comparison of the dynamic behavior of the controllers. Peaks in the error occur simultaneously in both strategies and correspond to the abrupt changes in the desired trajectory applied between 20 s and 40 s, with magnitudes being practically equal. Nonetheless, the FOPID demonstrates a significantly superior ability to correct the error. While the PID requires approximately 10 s to nullify the error after the reference change, the FOPID achieves the desired tracking within about 1 s. Overall, the PID controller exhibits an underdamped behavior with error overshoots and longer settling times. In contrast, the FOPID provides a faster and smoother response, effectively eliminating the error without notable overshoot.

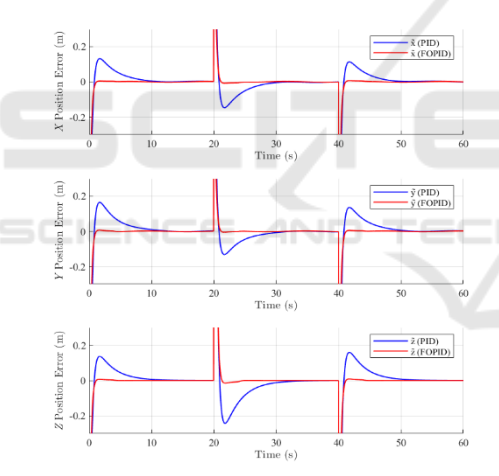


Figure 7: Position errors.

Figure 8 shows three of the seven control signals generated by each controller, corresponding to the linear velocities of the aerial manipulator. These signals are plotted within a ±2 m/s range to facilitate a clearer comparison of their dynamic differences. It can be observed that, at steady state, both control strategies reach similar values, indicating that the control signals converge to the same regime. However, during the transients caused by the reference changes at 20 s and 40 s, slight differences appear. The FOPID tends to generate smoother and less oscillatory signals, whereas the PID exhibits more abrupt responses, consistent with its less damped behavior observed in the position error.

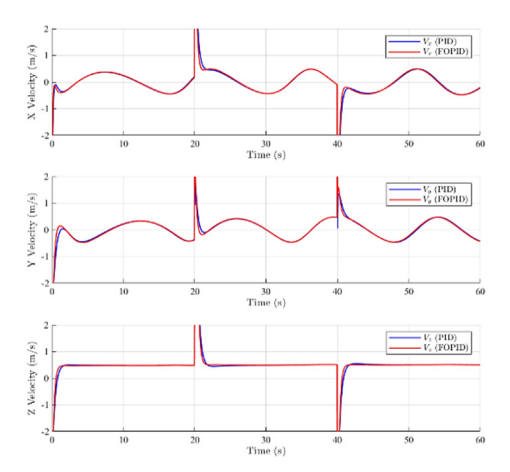


Figure 8: Linear velocity control signals.

5 DISCUSSION

The results obtained show that the FOPID controller implemented performs better than the PID controller, considering that the calibration parameters (proportional, derivative, and integrator) were the same for both controllers. Table 1 presents the performance indices ISE derived from the position errors in the three coordinates (x, y, z) for both controllers, along with the relative percentage improvement achieved by the FOPID. quantitative analysis reveals that the FOPID consistently reduces the ISE values across all coordinates, indicating more accurate tracking of the desired trajectory. On average, the FOPID improves performance by 21.27 %, relative to the PID, which supports its faster and smoother response, as also observed in the trajectories shown in Figure 6 and the error evolution in Figure 7.

Table 1: ISE Resulting ISE for Each Controller.

ISE	PID	FOPID	% Improvement
\tilde{x}	1.5526	1.1884	23.46%
ỹ	1.9318	1.4490	24.99%
ĩ	2.5807	2.1846	15.35%

These results validate the effectiveness of the fractional orders λ and μ in enhancing the dynamic behavior of the system by enabling finer tuning of the controller, particularly in scenarios involving abrupt changes in the reference trajectory. The implementation of the FOPID controller entails increased complexity in tuning, as it requires adjusting five parameters instead of the three used in the classical PID controller. To simplify this process,

an efficient sequential tuning strategy was applied: first, the PID parameters were tuned, followed by the optimization of the fractional orders. This approach reduces the search space and facilitates improved system performance. While these results confirm the efficacy of the kinematic approach under ideal conditions, it is acknowledged that its performance may degrade in scenarios where the payload or manipulator arm dynamics significantly influence the UAV's behavior. In such cases, future work should consider extending the approach to incorporate coupled dynamic models or robust control.

6 CONCLUSIONS

Based on the obtained results, it is evident that the FOPID controller demonstrated superior performance compared to the classical PID, achieving faster and more precise trajectory tracking with reduced oscillations. This improvement was also observed in response to abrupt changes in the reference trajectory, to which both controllers were subjected. The FOPID achieved a 21.27% improvement in the ISE compared to the classical PID. Although the FOPID requires tuning of five parameters compared to three in the classical controller, this provides greater flexibility in the adjustment process. Overall, the results validate the use of the FOPID as an efficient solution for trajectory tracking control of aerial manipulators under demanding conditions. Furthermore, since this control approach is model-free, it opens a future research avenue for aerial manipulators, focusing on robust and adaptive FOPID strategies to compensate for the complex dynamics of these robots.

As future work, we propose to extend the approach to schemes that incorporate coupled dynamics of the aerial manipulator, in order to evaluate how the dynamics of the arm affect the robotic system. The implementation of robust controllers based on FOPID will be analyzed.

ACKNOWLEDGEMENTS

The authors would like to express their sincere gratitude to the Escuela Politécnica Nacional for the financial support provided for research, development, and innovation through the project PIS-23-09: Artificial Intelligence Techniques Applied to an Aerial Manipulator in Semi-structured Environments. The authors also acknowledge the support from the Universidad de las Fuerzas Armadas ESPE through

the project PIEX-DACI-ESPE-24: Autonomous Control of Aerial Manipulator Robots. Finally, the authors are grateful to the ARSI and GIECAR research groups for their valuable theoretical contributions and technical support throughout the development of this work.

REFERENCES

- A. Faraj, M., & Mohammed Abbood, A. (2021). Fractional order PID controller tuned by bat algorithm for robot trajectory control. Indonesian Journal of Electrical Engineering and Computer Science, 21(1), 74. https://doi.org/10.11591/ijeecs.v21.i1.pp74-83
- Cajo, R., Mac, T., PLaza, D., Copot, C., Keyser, D., & Ionescu, C. (2019). A Survey on Fractional Order Control Techniques for Unmanned Aerial and Ground Vehicles. 66864–66878. https://doi.org/10.1109/AC CESS.2019.2918578
- Cao, G., Zhao, X., Ye, C., Yu, S., Li, B., & Jiang, C. (2022). Fuzzy adaptive PID control method for multi-mecanum-wheeled mobile robot. 2019–2029. https://doi.org/10.1007/s12206-022-0337-x
- Carvajal, C. P., Andaluz, G. M., Andaluz, V. H., Roberti, F., Palacios-Navarro, G., & Carelli, R. (2024). Multitask control of aerial manipulator robots with dynamic compensation based on numerical methods. Robotics and Autonomous Systems, 173, 104614. https://doi.org/10.1016/j.robot.2023.104614
- Delgado-Reyes, G., Valdez-Martínez, J. S., Guevara-López, P., & Hernández-Pérez, M. A. (2024). Hover Flight Improvement of a Quadrotor Unmanned Aerial Vehicle Using PID Controllers with an Integral Effect Based on the Riemann–Liouville Fractional-Order Operator: A Deterministic Approach. Fractal and Fractional, 8(11), 634. https://doi.org/10.3390/fractalfract8110634
- Ghamari, S., Narm, H., & Mollaee, H. (2022). Fractional-order fuzzy PID controller design on buck converter with antlion optimization algorithm. 340–352. https://doi.org/10.1049/cth2.12230
- Guayasamín, A., Leica, P., Herrera, M., & Camacho, O. (2018). Trajectory Tracking Control for Aerial Manipulator Based on Lyapunov and Sliding Mode Control. 36–41. https://doi.org/10.1109/INCISCOS .2018.00013.
- Leica, P., Camacho, O., Lozada, S., Guamán, R., Chávez, D., & Andaluz, V. H. (2017). Comparison of control schemes for path tracking of mobile manipulators. 28, 86–96. https://doi.org/10.1504/IJMIC.2017.085300
- Li, J., Chen, P., Chang, Z., Zhang, G., Guo, L., & Zhao, C. (2023). Trajectory Tracking Control of Quadrotor Based on Fractional-Order S-Plane Model. Machines, 11(7), 672. https://doi.org/10.3390/machines11070672
- Mohamed, M. J., Oleiwi, B. K., Abood, L. H., Azar, A. T., & Hameed, I. A. (2023). Neural Fractional Order PID Controllers Design for 2-Link Rigid Robot

- Manipulator. Fractal and Fractional, 7(9), 693. https://doi.org/10.3390/fractalfract7090693
- Moya, V., Espinosa, V., Chavez, D., Leica, P., & Camacho, O. (2016). Trajectory tracking for quadcopter's formation with two control strategies. 2016 IEEE Ecuador Technical Chapters Meeting (ETCM), 1–6. https://doi.org/10.1109/ETCM.2016.7750839
- Mundheda, V., Mirakhor, K., Rahul, K. S., & Govindan, N. (2023). Predictive Barrier Lyapunov Function Based Control for Safe Trajectory Tracking of an Aerial Manipulator. 1–6. https://doi.org/10.23919/ECC57647. 2023.10178336.
- Noordin, A., Mohd Basri, M. A., & Mohamed, Z. (2022). Position and Attitude Tracking of MAV Quadrotor Using SMC-Based Adaptive PID Controller. Drones, 6(9), 263. https://doi.org/10.3390/drones6090263
- Shah, P., & Agashe, S. (2016). Review of fractional PID controller. Mechatronics, 38, 29–41. https://doi.org/10.1016/j.mechatronics.2016.06.005
- Shao, K., Xia, W., Zhu, Y., Sun, C., & Liu, Y. (2025). Research on UAV Trajectory Tracking Control System Based on Feedback Linearization Control–Fractional Order Model Predictive Control. Processes, 13(3), 801. https://doi.org/10.3390/pr13030801
- Sharma, A., Gupta, S., Singh, S. P., Yadav, R. D., Song, H., Pan, W., Roy, S., & Baldi, S. (2025). Impedance and Stability Targeted Adaptation for Aerial Manipulator with Unknown Coupling Dynamics (arXiv:2504.01983). arXiv. https://doi.org/10.48550/ arXiv.2504.01983
- Suid, M. H., & Ahmad, M. A. (2022). Optimal tuning of sigmoid PID controller using Nonlinear Sine Cosine Algorithm for the Automatic Voltage Regulator system.
 128, 265–286. https://doi.org/10.1016/j.isatra.2021.11.037
- Timis, D. D., Muresan, C. I., & Dulf, E.-H. (2022). Design and Experimental Results of an Adaptive Fractional-Order Controller for a Quadrotor. Fractal and Fractional, 6(4), 204. https://doi.org/10.3390/fract alfract6040204
- Torvik, P. J., & Bagley, R. L. (1984). On the Appearance of the Fractional Derivative in the Behavior of Real Materials. Journal of Applied Mechanics, 51(2), 294–298. https://doi.org/10.1115/1.3167615
- Zhang, X., Xu, W., & Lu, W. (2021). Fractional-Order Iterative Sliding Mode Control Based on the Neural Network for Manipulator. Mathematical Problems in Engineering, 2021, 1–12. https://doi.org/10.1155/ 2021/9996719
- Zheng, W., Li, Z., Zhan, L., Xiu, B., Zhao, B., & Guo, Z. (2023). Robust fractional-order fast terminal sliding mode control of aerial manipulator derived from a mutable inertia parameters model. 2425, 012009. https://doi.org/10.1088/1742-6596/2425/1/012009